Hindawi
Mathematical Problems in Engineering
Volume 2023, Article ID 3536608, 13 pages
https://doi.org/10.1155/2023/3536608

Research Article

Design of Single Input Dual Output DC–DC Converter for Electric Vehicle Application

Sankara Kumar S[1] and Ramash Kumar K[2]

[1]Department of Electrical and Electronics Engineering, National Engineering College, Kovilpatti, Tamil Nadu, India
[2]Department of Electrical and Electronics Engineering, Dr. N.G.P Institute of Technology, Coimbatore-48, Tamil Nadu, India

Correspondence should be addressed to Ramash Kumar K; ramashkumar@drngpit.ac.in

Received 27 May 2023; Revised 18 October 2023; Accepted 19 October 2023; Published 14 November 2023

Academic Editor: Ciro Núñez-Gutiérrez

DC–DC converters are playing a vital in the electric vehicles (EVs) application. In current EVs, a separate DC–DC converter is used to charge both in the low voltage and the high-voltage batteries. These factors have resulted in higher output voltage ripples, higher switching and device conduction losses, all of which can have an impact on EV performance. In addition, the previous mulitport converters have more number of energy storage elements and switching devices for EV application. To address these issues, this article proposes a multiport DC–DC converter charging circuit for EVs. The proposed circuit has a single-input dual-output (SIDO) structure that consists of a positive output boost converter (POBC) with integration of buck converter (POBCIBC). Here, the POBC is used to stepping-up the voltage, while the buck converter is used to step-down the voltage. The POBC is a fundamental topology composed of Cascaded Boost Super Lift Luo Converters. The designed POBCIBC has several advantages such as reduced output voltage ripples, high-voltage transfer gain, proficient efficiency, lower switching and conduction losses, less number of storage components, and a compact structure over the existing multiport converters. The performance of the POBCIBC is tested at different operating conditions by constructing the MATLAB/Simulink and prototype models. The proposed converter has produced different output voltage levels based on their duty cycles variations. The results are presented to show the proficient POBCIBC for the EV application.

1. Introduction

Electric vehicles (EVs) can play a critical role in combating climate change around the world by lowering emissions and decreasing reliance on the fossil fuels. The main components of EVs are the battery, DC–DC converters, inverter, electrical machinery, battery management system (BMS), and control unit. The DC–DC converter is used to charge the battery in EVs while also increasing the high voltage from low-voltage renewable energy sources [1, 2]. However, in existing EVs, an individual DC–DC converter was used to charge both in the low voltage and the high-voltage batteries, which can result in increased switching losses, increased output voltage ripples, massive conduction losses, and a decrease in system efficiency. These issues affect the performance of the EVs. To solve these issues, this article introduces a single-input and multioutput (SIMO) DC–DC converter for EV. Positive output boost converter (POBC) with integration of buck converter (POBCIBC) in continuous conduction mode (CCM) with various duty cycles is considered as a SIMO converter for study in this article. In this article, the POBC is used for high voltage and the stepping down converter is used for low voltage. The POBCIBC outperforms existing EV battery charging multiport DC–DC converters in terms of voltage transfer gain (VTG), tenacity, and ripple voltage [3, 4]. The Luo converter with integration buck converter for EV application is well-executed [5]. However, the efficiency of this converter has produced 94.2%. The DC–DC converter fed small power rating of brushless DC motor drive for EV is well-presented [6]. However, the efficiency of the converter is low for this work. An enhanced deep learning method for driver detection and

Table 1: Comprehensive analysis of the proposed POBCIBC with previous converters for EV applications.

References	Number of Switches					VTG G_1	VTG G_2	Efficiency (%)
	Switch	Capacitor	Diode	Inductor	Total outputs			
[17]	2	3	3	2	2	$(2\text{-}1/1\text{-}d_2)$	$(d_1\text{-}d_2/1\text{-}d_2)$	98
[18]	2	6	6	2	2	$(1/1\text{-}d)$	(2/1-d)	93.98
[19]	1	5	2	2	2	$((1+\mathrm{N}_2)/(1\text{-}d)^2)$	$((2+N_2)/(1\text{-}d)^2)$	93.4
[20]	3	7	4	1	2	$(2(\mathrm{N}+1))/d_1$	$(1\text{-}d_3/d_1)$	92
[21]	1	3	4	2	1	$(1/1\text{-}d_1)$	–	90
[22]	1	4	4	1	3	$(2\text{-}d/1\text{-}d)$	$(\mathrm{d}N_b/1\text{-}d)$	92.5
[5]	1	4	2	2	2	(2/1-d)	$(1/1\text{-}d)$	94.2
Proposed POBCIBC	2	2	2	2	2	$1/1\text{-}d_2$	$(d_1\text{-}d_2/1\text{-}d_2)$	99.39

assistance EV with proficient performance has been presented [7].

Multi-input and multi-output (MIMO) DC–DC converters are currently hot topics in EVs. SIMO transformer based DC–DC converter with varying output voltage is well-executed [8]. However, this converter had a number of issues such as big transformer size, higher cost, and more quantity of power switches, higher on–off losses, and a complex control as well as driver circuit, which can reduce their efficiency. The SIMO with coupled inductor is well-presented [9]. A soft switching based SIMO converter has been reported in [10]. However, from these woks, the coupled inductors have resulted in more leakage current, more on–off losses and complex design steps. The modified buck–boost DC–DC converter has been systematically addressed [11]. According to this article, the converter is designed for small power applications by using three switches with hard switching concepts to compute the lower and maximum surge inductor currents.

Design of sliding mode controller (SMC) for multiphase charger and discharger bidirectional DC–DC converters have been well-reported [12]. From this work, the inductor current of this converter with this control has produced a ripple current of 1.58 A and peak overshoots of 1 V during the load variations. Furthermore, the structure of the designed converter has more complex, and charged only a single battery. The zero voltage switching (ZVS) DC–DC converter using IC UCC389 control for low-voltage battery charging in EV is well-presented [13]. However, the designed converter has charged single battery with a complex structure and produced conduction losses of 20 W. Furthermore, the cost of phase shifter IC is excessive due to increased power losses. A real-time analysis of a five-stage DC–DC boost converter with a series LC for EVs is well-presented [14]. However, this converter has more storage elements (like 10 capacitors, and one inductor) and 8 diodes. Similarly, the output voltage of this converter has generated peak overshoots of 34.9% and a settling time of 100 ms. The performance of various DC–DC converters with their control methodologies for EVs has been reviewed, and their parameters have been recorded in [15]. Based on these analyses, the converter efficiency ranges starts from 61.8% to 92.1% with a single battery. An improved current-operated bidirectional power converter for EV battery charging has been discussed [16]. But, this converter has charged a single battery with moderate efficiency. The Super Lift Luo Converter with buck converter integration for EV has been discussed [17]. However, this converter has produced an efficiency of 98% with two switches, two inductors, three capacitors, and three diodes. Table 1 indicates the comprehensive analysis of the proposed POBCIBC with previous converters research gaps for EV applications. From these works, it is evident that the proposed POBCIBC has produced efficiency of 99.39% with minimum number of elements over the existing converters.

According to the literature review, no design of POBCIBC with duty cycle control for EV battery charging application has been reported.

Therefore, in this article, it is to design the POBCIBC for EV application. The complete model is validated at various working conditions by making the MATLAB/Simulink and the prototype models.

The following is the main objectives of this article:

(i) First, the VTG and design equations for components of the POBCIBC are derived, and then the duty cycles for the converter are varied to achieve a wide range of regulated output voltages.

(ii) Next, the POBCIBC is tested at different duty cycles and load resistance variations by constructing the Simulink and the experimental models.

(iii) Finally, the results of proposed converter has analyzed via. time domain specification, output voltage ripples, and efficiency analysis at different converter parameter variations.

This article is organized as follows: Section 1 discusses the introduction, literature review, and main objectives of this article. Sections 2 and 3 discuss the operation and mathematical VTG of POBCIBC. Section 4 presents the proposed converter components designs formulas. Section 5 performs the efficiency calculation. Section 6 contains the results and discussions of POBCIBC at different operating conditions. Conclusions and future works are listed in Section 7.

2. Proposed POBCIBC Working

The POBCIBC for EV application is illustrated in Figure 1. It includes input voltage V_{in}, two MOSFET switches S_1, S_2,

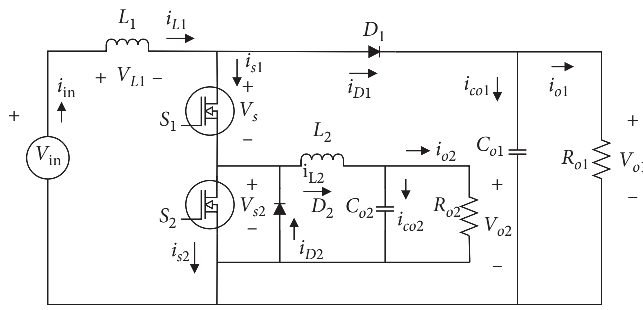

FIGURE 1: Structure of the proposed POBCIBC.

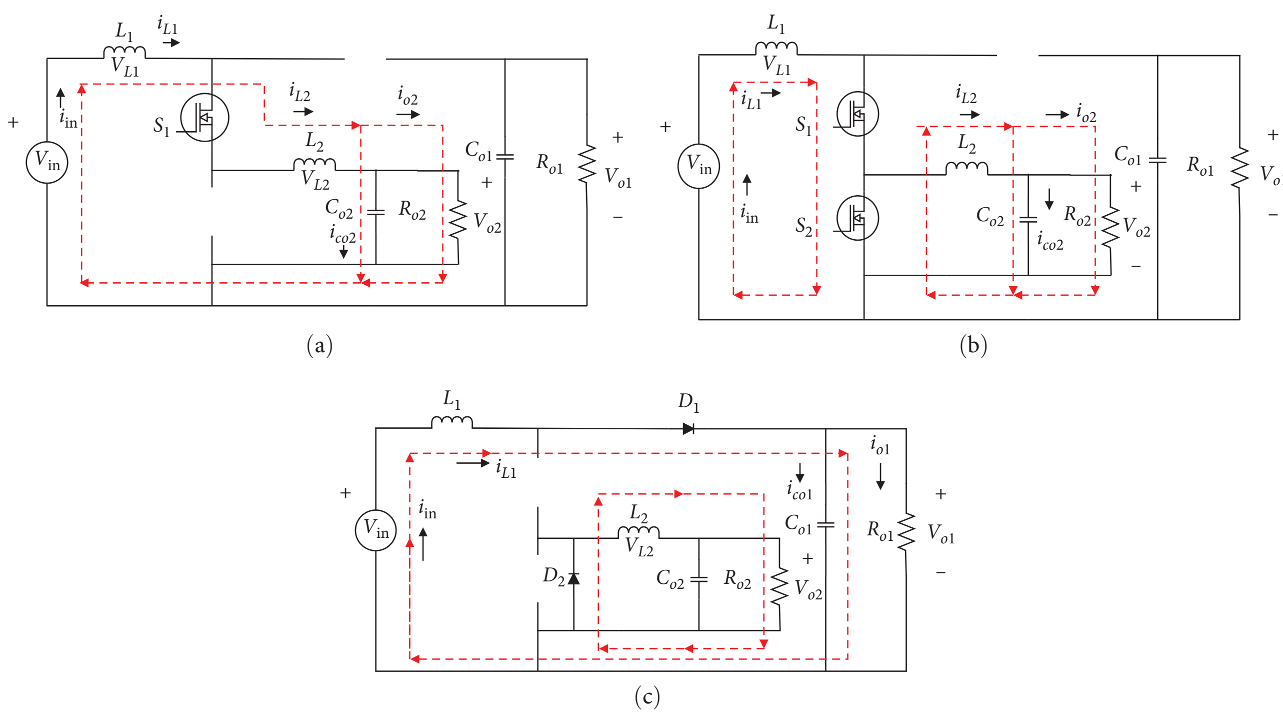

FIGURE 2: Modes of operation of proposed POBCIBC, (a) Modes 1 and 3, (b) Mode 2, and (c) Mode 4.

storage components such as inductors (L_1, L_2)/capacitor (C_{o1}, C_{o2}), power transfer diodes D_1, D_2 and load resitances R_{o1}, R_{o2}. The main aids of the POBCIBC has single input and two output voltage at different levels. This POBCIBC is more suitable for power source in various components of EV. The output voltage (V_{o1}) of POBCIBC has been improved by using boost converter whereas the low-output voltage voltage (V_{o2}) of it can be generated with the help of buck converter. The POBCIBC has good VTG, reduced circuit components, minimized current and voltage ripples, simple strucure, good power density and efficiency in comaprion with tradtional multiport converters, and KY converters and SEPIC. The working of the POBCIBC is divided into four modes of operation and its equivalent circuits are represented in Figure 2(a)–2(c).

Mode 1 ($0 < t < t_1$) (Refer Figure 2(a)): During the Mode 1 operation, S_1 is closed and S_2 is open. The stored energy in the previous mode of inductor L_1 is de-energized to energize the inductor L_2 in this mode and to supply the buck load R_{o2}. This mode is completes after the $(d_1\text{-}d_2/2)T_s$ time interval. The S_1 voltage is zero due to the resonance path between the L_1, L_2, and C_{o2} in the earlier switching state time interval. Besides, the D_1 and D_2 are in reverse polarized mode.

$$V_{s1/s2/D1/D2-\text{stress}} = V_{o1} - V_{\text{in}}. \tag{1}$$

Mode 2 ($t_1 < t < t_2$) (Refer Figure 2(b)): In Mode 2 operation, S_1 is open and S_2 is closed. The stored energy in the inductor L_2 is released energy to load R_{o2}. In addition, L_1 is energized with V_{in}. The D_2 is inverse polarized in this mode. The time interval for this mode is d_2T_s time interval.

$$\begin{aligned} i_{s1/s2-\text{stress}} &= i_{\text{in}} \\ i_{D1-\text{stress}} &= i_{o1} \\ i_{D2-\text{stress}} &= i_{o2} \end{aligned} \tag{2}$$

Mode 3 ($t_2 < t < t_3$) (Refer Figure 2(a)): The operation in this mode is same as that of Mode 1.

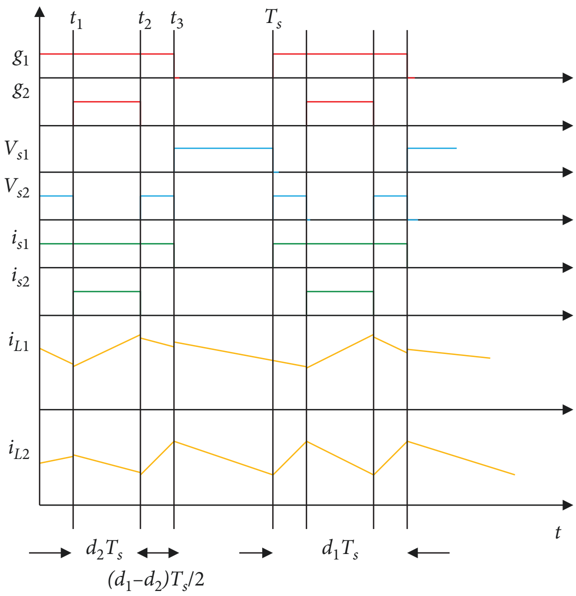

Figure 3: Switching pattern, voltage, and current waveforms for various elements of POBCIBC.

Table 2: Specification of POBCIBC for EV application.

Name of the parameters	Symbols	Value	
Duty cycles	d_1	0.6	0.9
	d_2	0.3	0.8
Input voltage	V_{in}	12 V	12 V
Output voltages	V_{o1}	17.14 V	60 V
	V_{o2}	5.14 V	6 V
Load resistances	R_{o1}	25 Ω	
	R_{o2}	12.5 Ω	
Load currents	i_{o1}	0.6856 A	2.4A
	i_{o2}	0.4112 A	0.48A
Input current	i_{in}	0.985 A	13.633A
Efficiency	η	99.39%	89.78%
Output powers	$P_{o1}+P_{o2}$	11.75 W	146.88 W
Input power	P_{in}	11.82 W	163.5 W
Switching frequency	f_s	30 kHz	
Inductors	L_1 and L_2	3.2 and 2 mH	
Output capacitors	$C_{o1}=C_{o2}$	3 μF	
Capacitors ripple voltage	ΔV_{co1} and ΔV_{co2}	1 and 0.1 V	

Mode 4 ($t_3 < t < t_4$) (Refer Figure 2(c)): In this mode, S_1 and S_2 are in open states. The L_1 and L_2 is released energy to supply the loads R_{o1} and R_{o2}.

$$\begin{aligned} V_{o1} &= V_{in} - V_{L1} \\ V_{o2} &= -V_{L2} \\ I_{L1} &= i_{co1} + V_{o1}/R_{o1}. \end{aligned} \tag{3}$$

Gate pulses, voltage, and current key waveforms for the different components of POBCIBC are illustrated in Figure 3. The parameters of POBCIBC are cataloged in Table 2.

3. Mathematical Computation of VTG of POBCIBC

For computing the VTG of POBCIBC, assuming that the proposed converter has ideal components and minimal ripples for the inductors potential. The VTG of the POBCIBC is derived from the modes of operation of it and also depends on the voltage-second balancing of inductors. The VTG for step-up output of boost converter is arrived as Equation (4).

$$\begin{aligned} V_{in}d_2T_s &= [(V_{o1} - V_{in}) \times (1-d_2)]T_s \\ V_{in}d_2 &= V_{o1} - V_{in} - V_{o1}d_2 + V_{in}d_2 \\ V_{in} &= V_{o1}(1-d_2) \\ G_1 &= V_{o1}/V_{in} = (1/1-d_2). \end{aligned} \tag{4}$$

Likewise, VTG of the step-down output of buck converter is engraved as Equation (5)

$$\begin{aligned} V_{o2}d_2 &= [(d_2-d_1) + (d_1-d_2) \times (1/1-d_2)]V_{in} \\ V_{o2}d_2 &= ([(d_2-d_1)x(1-d_2) + (d_1-d_2)]/(1-d_2))V_{in} \\ V_{o2}d_2 &= ([d_2 - d_2^2 - d_1 + d_1d_2 + d_1 - d_2]/(1-d_2))V_{in} \\ G_2 &= V_{o2}/V_{in} = (d_1 - d_2/1-d_2). \end{aligned} \tag{5}$$

The VTG (G_1) of POBC output voltage depends on duty cycle d_2, whereas the VTG (G_2) of buck output is a function of d_1 and d_2. The graphical representation of theoretical analysis of the proposed converter is depicting in Figure 4. It is more suitable for EV due to utilizing the different ranges of output voltages. From the Figure 4, $0 < d_1 < 0.9$, $0 < d_2 < 0.9$, the VTGs are redefined as Equations (6) and (7)

$$V_{in} < V_{01} < 10\ V_{in}, \tag{6}$$

$$0 < V_{02} < 0.8\ V_{in}. \tag{7}$$

4. Design of Circuit Components of POBCIBC

This part deals about the circuit components of the POBCIBC. The inductors, L_1 and L_2 decide the switch current stress and output current ripples [17]. Therefore, designing the optimal ranges of inductors plays a significant role. Figure 4 show the inductor peak-to-peak current ripple is evaluated by Equation (8).

$$\Delta i_{L1} = V_{in}d_2/L_1f_s. \tag{8}$$

The linear decreasing of inductor peak-to-peak current ripple L_2 (see Figure 4) is obtained by Equation (9).

$$\Delta i_{L2} = V_{o2}(1-d_1)/L_2f_s. \tag{9}$$

The preferred ranges of L_1 and L_2 are evaluated using the Equations (8) and (9).

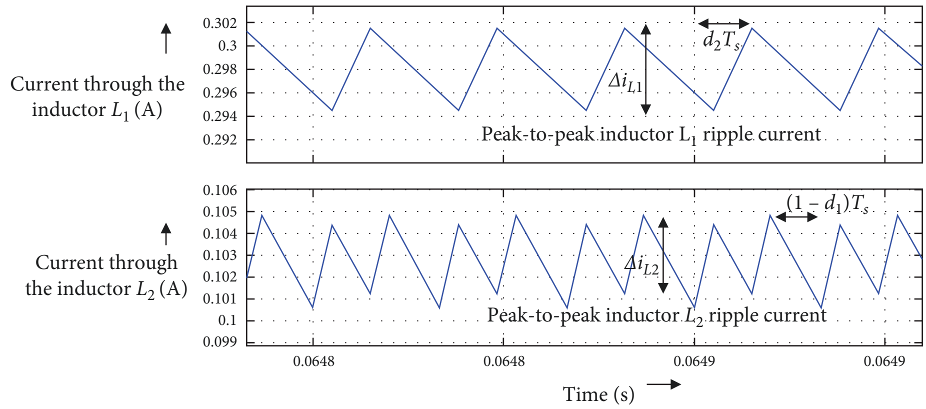

FIGURE 4: Peak-to-peak inductor current ripples L_1 and L_2 of POBCIBC.

Next, the proper ranges of filter capacitors of POBCIBC are obtained by using Equation (10).

$$\Delta V_{co} = \Delta q / C_o \tag{10}$$

where ΔV_{co} is peak-to-peak capacitor ripple voltage and Δq is charge.

Hence, the output capacitors are computed [17] with help of the Equation (11).

$$\begin{aligned} C_{o1,\min} &\geq V_{\text{in}}(1-d_1)_{\max}/\Delta V_{co1} L_1 f_s, \\ C_{o2,\min} &\geq V_{\text{in}}(d_2-d_1)_{\max}/\Delta V_{co2} L_2 f_s. \end{aligned} \tag{11}$$

Using Equation (11) at fixed switching frequency, the minimal ranges of C_{o1} and C_{o2} are mainly affected by d_1, d_2, and V_{in}. In addition, the voltages stresses of S_1, S_2, D_1, D_2, and D_3 computed with help of the Equation (12).

$$V_{s1/s2/D1/D2-\text{stress}} = V_{o1} - V_{\text{in}}. \tag{12}$$

Also, the current stresses of the devices are evaluated by Equation (13) with assuming free ripple of the inductors of this converter.

$$\begin{aligned} i_{s1/s2-\text{stress}} &= i_{\text{in}} \\ i_{D1-\text{stress}} &= i_{o1} \\ i_{D2-\text{stress}} &= i_{o2}. \end{aligned} \tag{13}$$

5. Efficiency Computation

The element losses are considered when calculating the converter efficiency. It is written as Equation (14).

$$\eta = P_o/(P_o + P_{\text{Losses}}). \tag{14}$$

The overall power losses of the converter are then expressed as Equation (15).

$$P_{\text{Losses}} = P_{\text{Switches}} + P_{\text{Diodes}} + P_{\text{Capacitors}} + P_{\text{Inductors}}. \tag{15}$$

The switching power losses are calculated during on and off conditions

$$P_{\text{Switches}} = P_{S,\text{on}} + \left(P_{S,\text{off}/2}\right). \tag{16}$$

Using the Equations (17)–(20), the switching power losses in on/off operating conditions are evaluated.

$$P_{S1,\text{on}} = r_{\text{on}}\left[(i_{\text{in}}^2 - i_{02}^2)d_2 + i_{o2}d_1 + 2i_{o2}i_{\text{in}}\sqrt{d_1}d_2 - d_2\right], \tag{17}$$

$$P_{S2,\text{on}} = r_{\text{on}} i_{\text{in}}^2 d_2, \tag{18}$$

$$P_{S,\text{off}} = f_{sC_{os}} V_{S-\text{stress}}^2, \tag{19}$$

$$P_{S1\&S2,\text{off}} = f_{sC_{os}} (V_{o1} - V_{\text{in}})^2, \tag{20}$$

Diode conduction and nonconduction state losses are calculated with help of Equations (21) and (22).

$$P_{D1,\text{on}} = r_f i_{\text{in}}^2 (1 - d_1), \tag{21}$$

$$P_{D1,\text{off}} = V_f i_{\text{in}} (1 - d_1), \tag{22}$$

where r_f is diode forward resistance and V_f is threshold or forward voltage of the diode.

$$\text{Total diode losses, } P_{\text{Diodes}} = P_{D1,\text{on}} + P_{D1,\text{off}}. \tag{23}$$

Storage elements power losses are computed by using Equations (24) and (25).

$$P_{\text{Inductors}} = r_1\left(i_{\text{in}}\sqrt{1-d_2} + i_{01}\sqrt{d_2}\right)^2 + r_1\left(i_{o1}\sqrt{d_1-d_2}\right)^2, \tag{24}$$

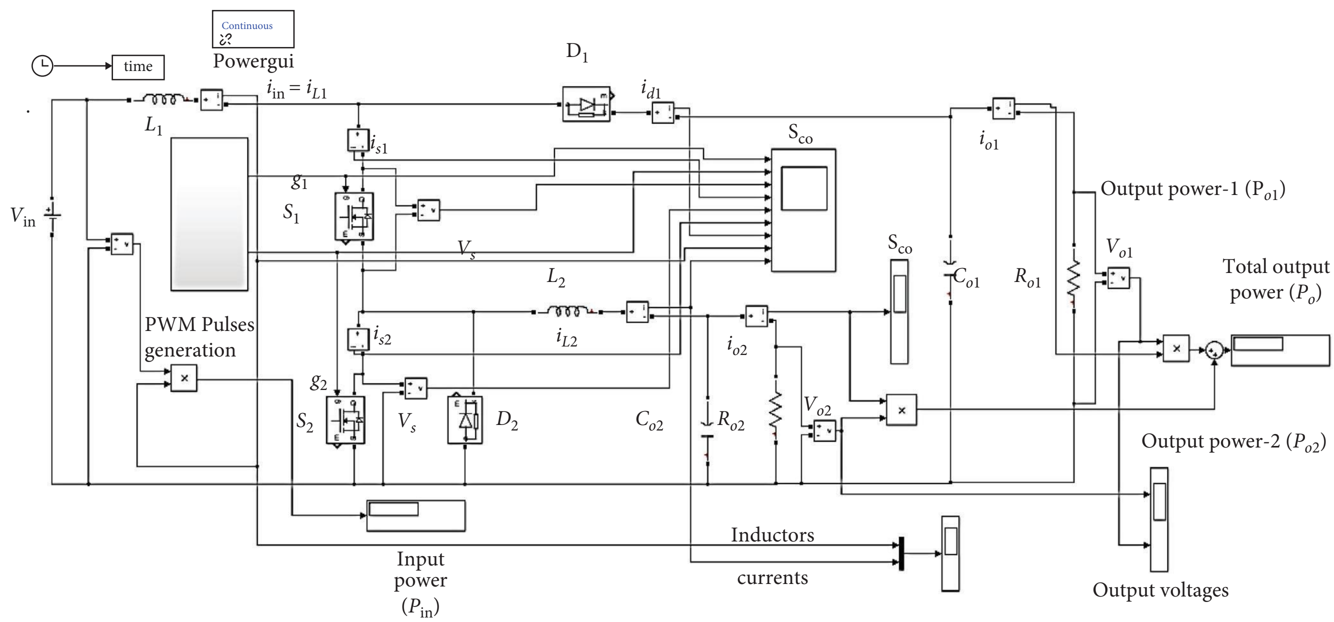

(a)

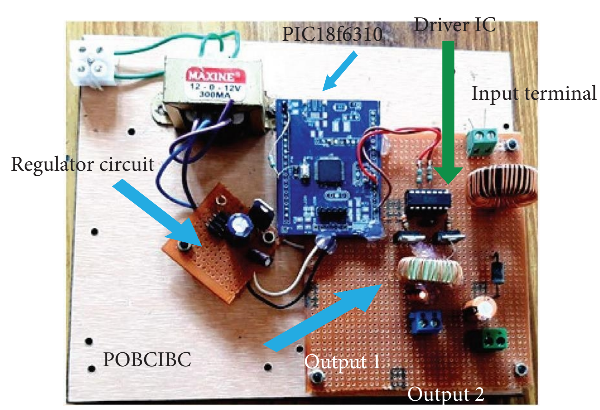

(b)

FIGURE 5: Proposed POBCIBC, (a) MATLAB/Simulink model and (b) prototype model.

$$P_{\text{Capacitors}} = r_2\left(\left(i_{\text{in}} - i_{o1}\right)\sqrt{1 - d_2} + i_{01}\sqrt{d_2}\right)^2 + r2\left(\left(i_{\text{in}} - i_{o1}\right)\sqrt{d_1 - d_2} + i_{o2}\sqrt{1 + d_2 - d_1}\right)^2, \tag{25}$$

where r_1 is internal resistance of inductors and r_2 is internal resistance of capacitors.

6. Results and Discussions

This section describes the simulation and experimental responses of the POBCIBC for EV applications at various load operating conditions, with the specifications of the same converter cataloged in Table 2. The following are the specifications of the converter circuit: MOSFTE IRFN 540 switches S_1_S_2, diodes, D_1, D_2-UF5803, inductors, L_1, L_2-Ferrite core (10 A), capacitors, C_{o1}, C_{o2} -electrolytic type, pulse width modulation (PWM) generation using microcontroller PIC 18f6310 (32 MHz, PC1, and PC2) and driver IC-Fan 6832 with amplification circuit. Figure 5(a) depicts the Simulink model of the POBCIBC, while Figure 5(b) depicts the prototype model of the same converter. The PWM pulses for switches of the converter are generated by using the PIC18f6310. Then, it is applied to the Fan 6832 driver circuit to provide isolation between the power and control units. The driver IC outputs are then connected to the gate and source of the switches S_1 and S_2 to regulate the output voltages with different duty cycles.

Figures 6(a) and 6(b) depict the simulated and experimental responses of the output voltages, V_{in}, and PWM pulses of the proposed POBCIBC with $V_{\text{in}} = 12$ V and duty cycles of switches $d_1 = 60\%$ and $d_2 = 30\%$. From these figures, it is clearly found that the POBCIBC output voltages have $V_{o1} = 17.14$ V and $V_{o2} = 5.14$ V matched theoretical values (refer Table 2) with small overshoots and a quick setting time of 0.001 s. In addition, output voltages of the proposed

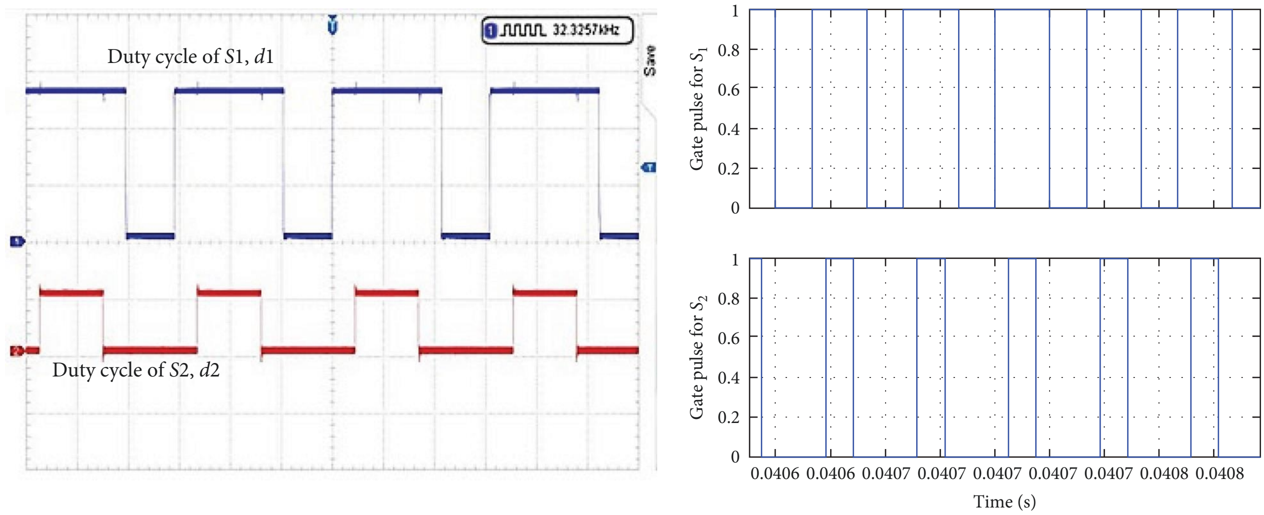

(a)

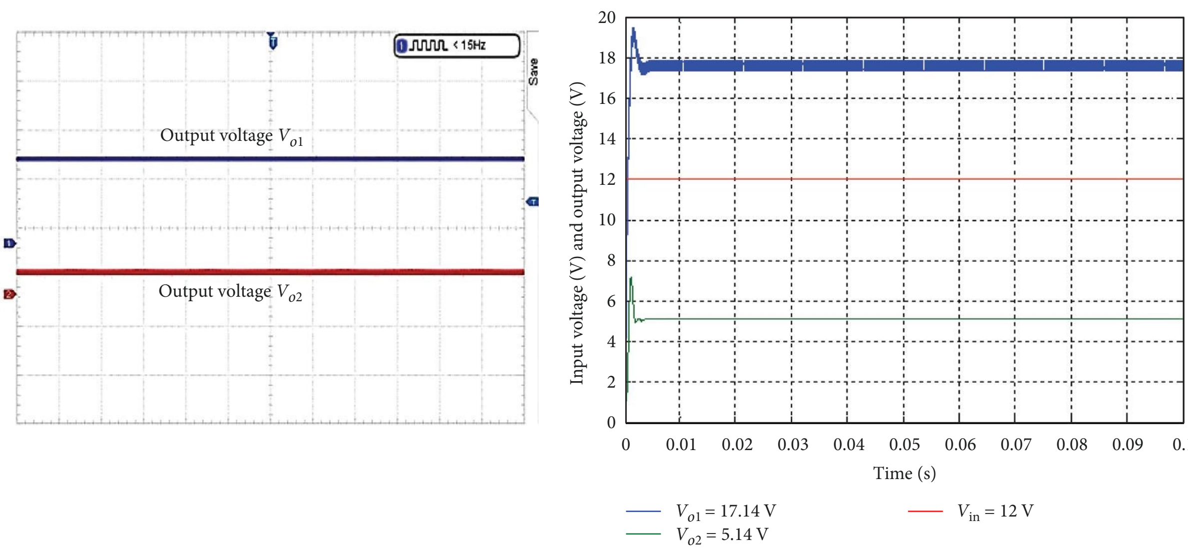

(b)

Figure 6: Simulated and experimental results of POBCIBC, (a) $d_1 = 60\%$ and $d_2 = 30\%$ (CH1 : 2 V/div; CH2 : 5 V/div-gate voltages of switches) and (b) input voltage and output voltages (CH1 : 10 V/div; CH2 : 10 V/div-output voltages; time: 20 μs/div).

converter has produced little ripples in both the experimental and the simulation responsess. Figures 7(a) and 7(b) show the experimental and simulation responses of the output voltages, input voltage, and PWM pulses of the proposed POBCIBC with $V_{\text{in}} = 12$ V and $d_1 = 90\%$ and $d_2 = 80\%$. From these figures, it is clearly observed that both the experimental and the simulation responses of output voltages of the POBCIBC have $V_{\text{o1}} = 60$ V and $V_{\text{o2}} = 6$ V, negligible overshoots and a setting time of 0.02 s. Furthermore, the V_{o1} and V_{o2} of the proposed converter have produced little ripples in both experimental and simulation analysis. Theoretical values (Table 2) are closely matched to both in the experimental and the simulation results.

Figures 8(a) and 8(b) depict the POBCIBC simulated gate pulses, voltage across the switches, and current through the switches/inductors/diodes responses with $V_{\text{in}} = 12$ V and $d_1 = 60\%$ and $d_2 = 30\%$ at different load resistance. It is found that the voltage across the switches, current through the switches, inductor, and diodes of the designed POBCIBC has no voltage and current stresses during the converter operation.

The POBCIBC was also operating in CCM/discontinuous conduction mode (DCM) because the inductor currents were continuous. All of the parameters correspond to the theoretical key waveform (see Figures 3 and 8). The performance of POBCIBC at rated load conditions is recorded in both the simulated and the experimental numerical results in Table 3. From theses result, it is evident that the proposed POBCIBC has produced efficiency of 99.39% (simulation) and 98.49% (experimental) at load of $R_{\text{o1}} = 25\,\Omega$ and $R_{\text{o2}} = 12.5\,\Omega$ and minimum ripples of the output voltages (1.2 V (simulation), 1.6 V (experimental) and 0.005 V (simulation), 0.0007 V

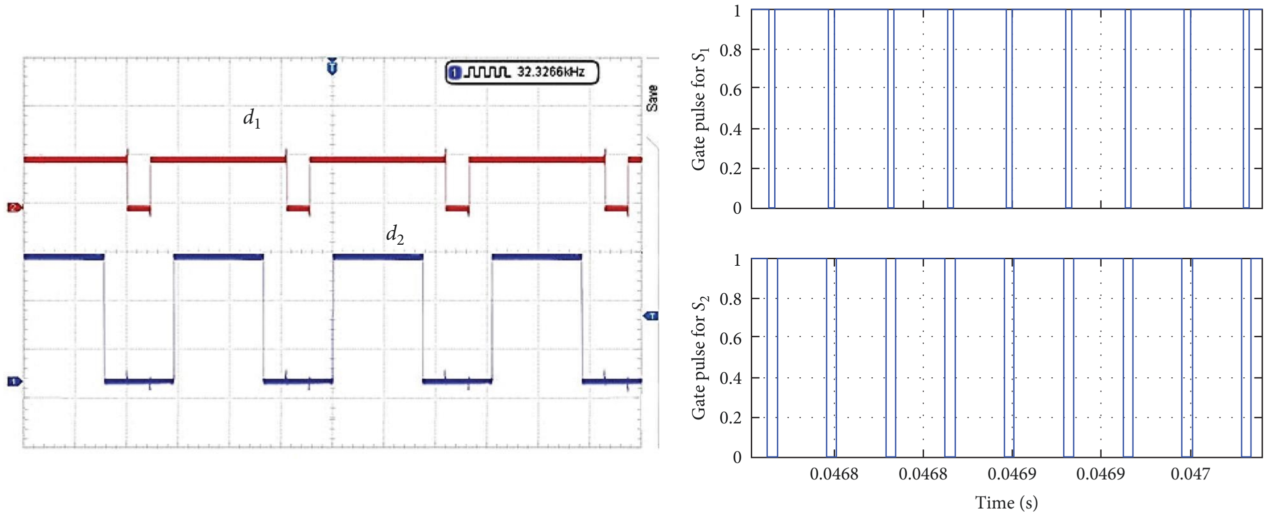

(a)

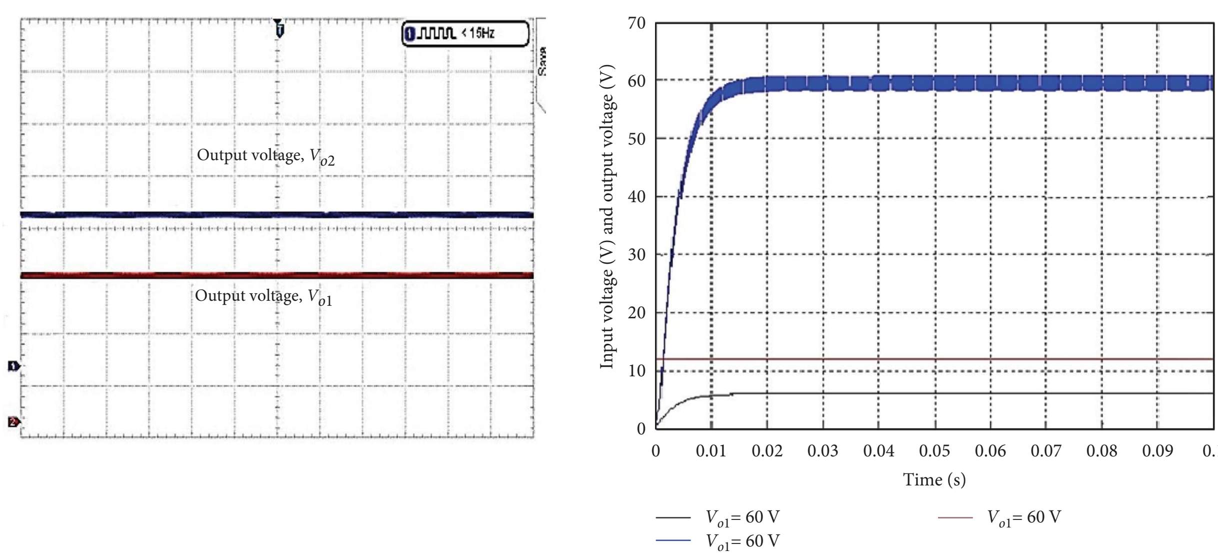

(b)

FIGURE 7: Simulated and experimental results of POBCIBC, (a) $d_1 = 90\%$ and $d_2 = 80\%$ CH1 : 2 V/div; CH2 : 5 V/div-gate voltages of switches) and (b) input voltage and output voltages (CH1 : 10 V/div; CH2 : 20 V/div-output voltages; time: 20 μs/div).

(experimental)) with duty cycles of switches $d_1 = 0.6$ and $d_2 = 0.3$.

Tables 1 and 3 indicate the comprehensive analysis of the proposed POBCIBC with previous converters for the EV applications. From these works, it is evident that the proposed POBCIBC has produced efficiency of 99.39% (see Table 3 highlighted in bold) with minimum number of elements over the existing converters.

The percentages of loss breakdown at nearly full load for various POBCIBC components are shown in Figure 9 using Equations (14)–(25). As a result, power losses are dominated by semiconductor device losses. It should be noted that the conduction loss of the switches and diodes becomes dominant due to the high current flow through them in the high-voltage gains and output powers. As a result, high-power semiconductors with low on-resistance should be used to improve the efficiency of the same converter. Figure 10(a)–10(d) depicts the experimental voltage across the S_1 and S_2, and current through the inductor (i_{L2}), and I_{D1} responses for POBCIBC with $V_{\text{in}} = 12$ V and $d_1 = 60\%$ and $d_2 = 30\%$ at rated load. From these results, it is found that the voltage across the switches, current through the inductor and the diode of the same converter has no voltage and current stresses during the POBCIBC operation. Therefore, the designed converter has more efficiency for EV application.

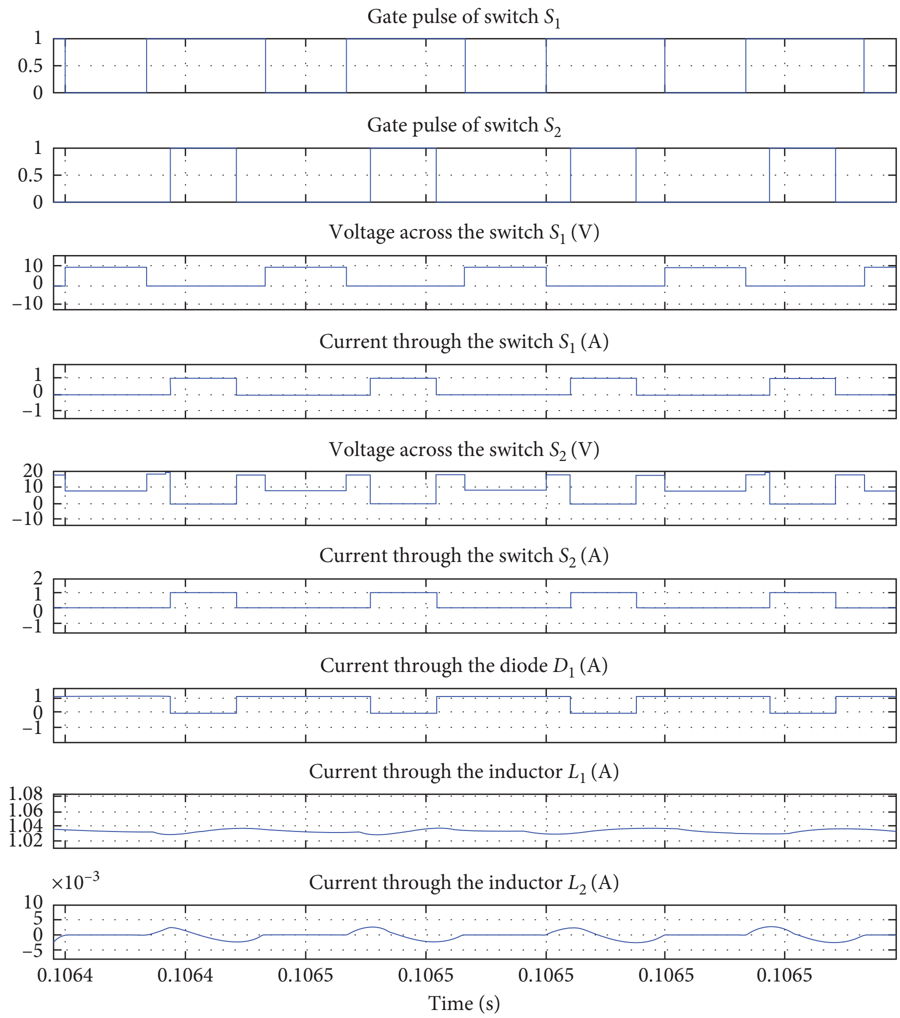

(a)

Figure 8: Continued.

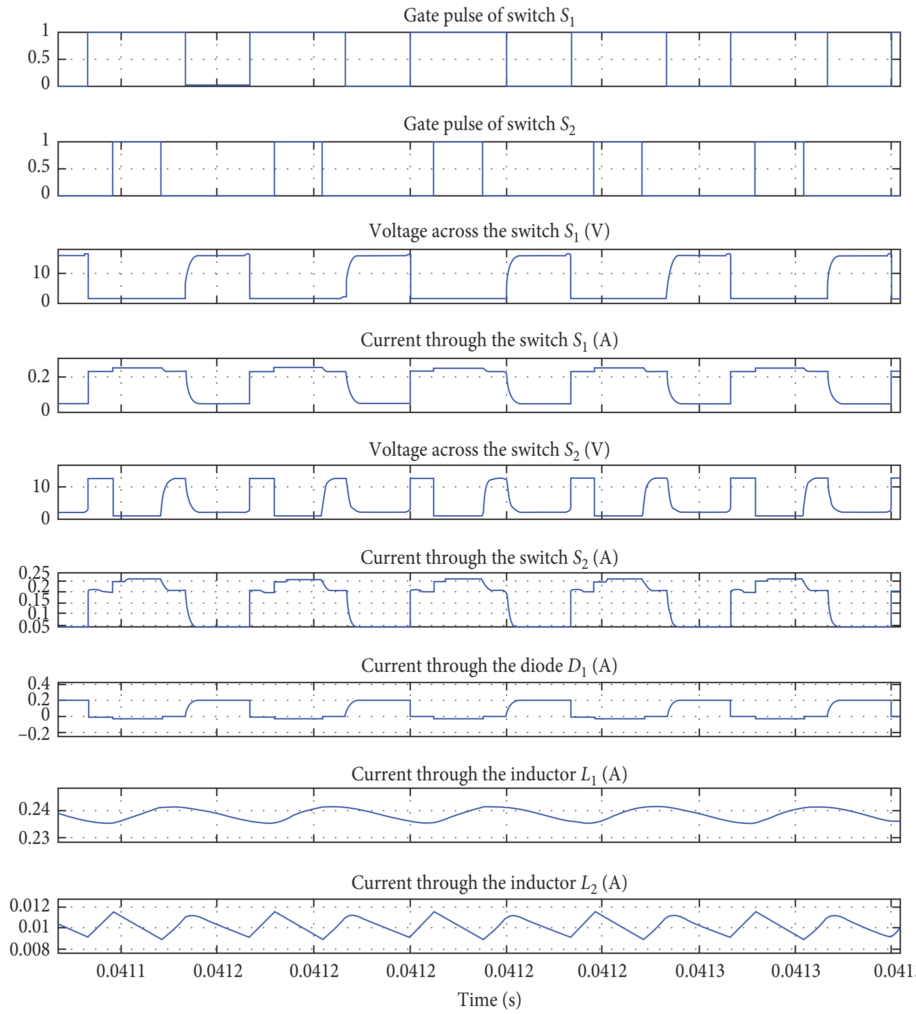

(b)

Figure 8: (a) Simulated current and voltage variations waveform for various elements of proposed POBCIBC ($R_{o1} = 25\,\Omega$ and $R_{o2} = 12.5\,\Omega$). (b) Simulated current and voltage variations waveform for various elements of proposed POBCIBC ($R_{o1} = 100\,\Omega$ and $R_{o2} = 50\,\Omega$).

Table 3: Simulated and experimental performance analysis of POBCIBC for EVs application at rated load operating condition with $V_{in} = 12$ V and duty cycles of $d_1 = 60\%$ and $d_2 = 30\%$.

R_{o1} (Ω)	R_{o2} (Ω)	Efficiency η (%)		Ripple output voltage V_{o1} (V)		Ripple output voltage V_{o2} (V)	
		Simulated	Experimental	Simulated	Experimental	Simulated	Experimental
25	**12.5**	**99.39**	**98.49**	**1.2**	**1.6**	**0.0005**	**0.0007**
50	25	95.48	94.58	1	1.2	0.001	0.0015
100	50	91.22	90.33	0.7	0.95	0.002	0.0026
150	75	87.98	86.88	0.5	0.66	0.003	0.0035
200	100	85.11	84.22	0.25	0.34	0.004	0.0044
250	125	82.49	81.33	0.2	0.32	0.005	0.0053

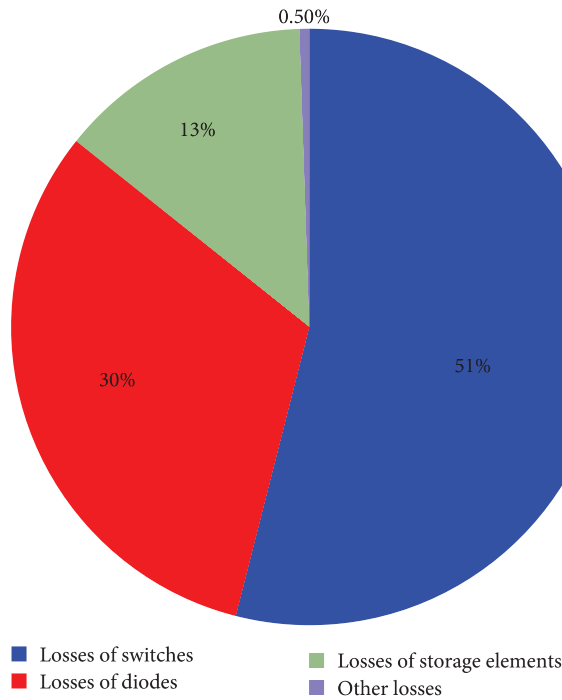

FIGURE 9: Distribution of experimental losses in POBCIBC at rated load conditions.

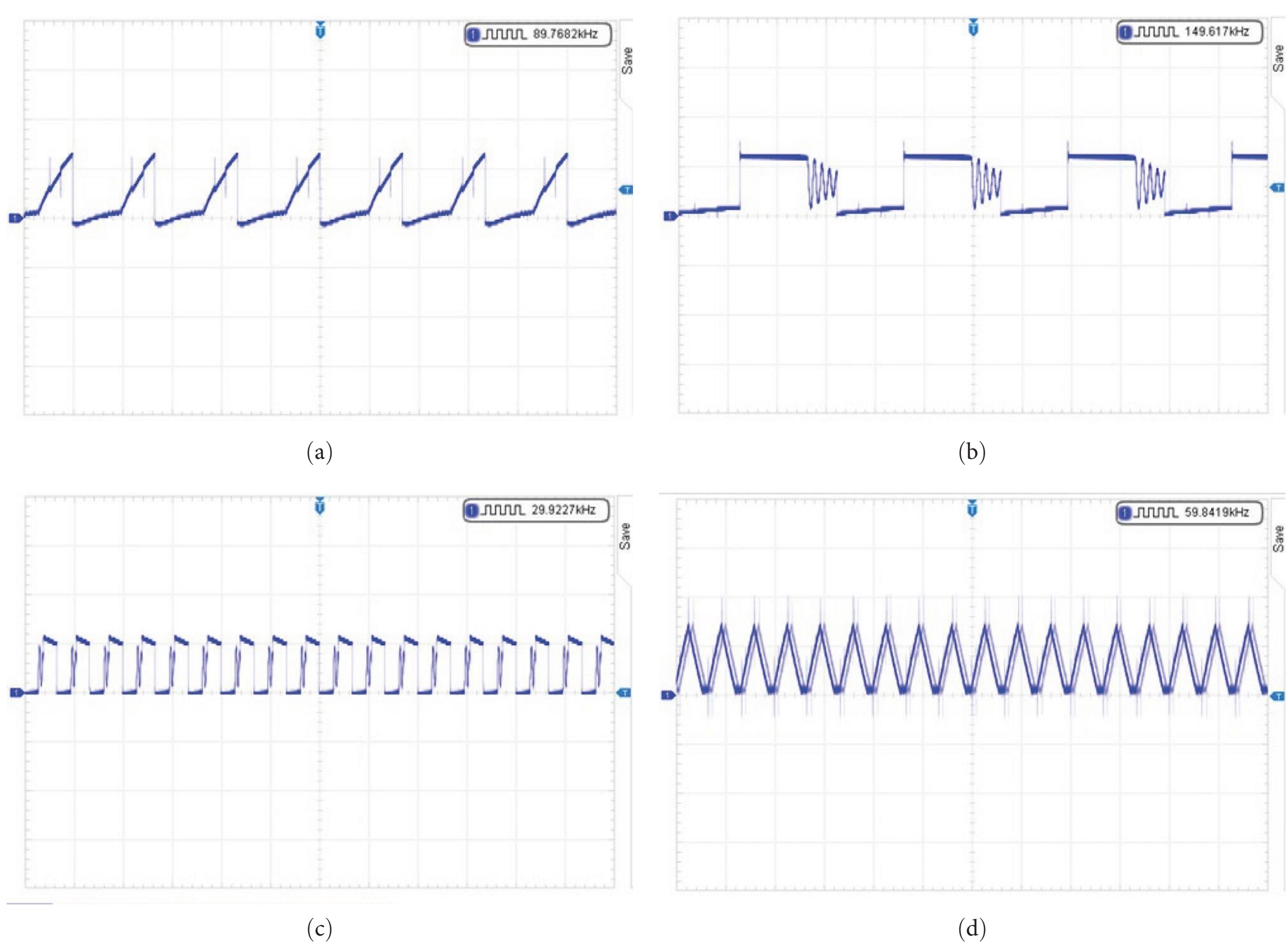

FIGURE 10: Experimental current and voltage variations responses for various elements of proposed POBCIBC ($R_{o1} = 25\,\Omega$ and $R_{o2} = 12.5\,\Omega$ $V_{in} = 12$ V and $d_1 = 60\%$ and $d_2 = 30\%$) (a) voltages across switch S_1 (CH1 : 20 V/div), (b) voltages across switch S_2 (CH1 : 10 V/div), (c) current through diode D_1 (CH1 : 1 A/div) and (d) current through inductor L_2 (CH1 : 500 mA/div).

7. Conclusions

In this article, the theoretical analysis, design and output voltage regulation of multiport POBCIBC operated in CCM using different duty cycle has been successfully demonstrated. The PWM pulses were generated using PIC18f6310 for POBCIBC. The main merits of the designed POBCIBC over the previous multiport converter as follows:

(i) Obtain the good VTG and flexibility to change the different output voltages;
(ii) Excellent efficiency like 99.39%;
(iii) Minimal output ripple voltages as well as inductor ripple currents;
(iv) Simple structure and less number of components; and
(v) Low conduction and switching losses.

The experimental and simulation results are presented in order to prove the competence of the designed multiport POBCIBC at different load and duty cycle operating conditions. It is, therefore, mainly designed for EV battery charging application.

In future, multiport converter based LUO and KY topologies to be built for EV and renewable energy applications.

Data Availability

The data are used to support the findings of this study are included within the article.

Disclosure

It was performed as a part of the Employment of Ramash Kumar K, Department of Electrical and Electronics Engineering, Dr. N.G.P. Institute of Technology, Coimbatore-48, Tamilnadu, India.

Conflicts of Interest

The authors declare that they have no conflicts of interest.

References

[1] S. Habib, M. M. Khan, F. Abbas et al., "Contemporary trends in power electronics converters for charging solutions of electric vehicles," *CSEE Journal of Power and Energy Systems*, pp. 1–36, 2020.
[2] A. Alahyari, M. Fotuhi-Firuzabad, and M. Rastegar, "Incorporating customer reliability cost in PEV charge scheduling schemes considering vehicle-to-home capability," *IEEE Transactions on Vehicular Technology*, vol. 64, no. 7, pp. 2783–2791, 2015.
[3] B.-R. Lin, "DC–DC converter implementation with wide output voltage operation," *Journal of Power Electronics*, vol. 20, pp. 376–387, 2020.
[4] F.-L. Luo and Y. Hong, *Advanced DC/DC Converters*, PCRC Press and Taylor and Francis Group, London, New York, 2006.
[5] S. K. Ramu, R. K. Balaganesh, S. K. Paramasivam et al., "A novel high-efficiency multiple output single input step-up converter with integration of Luo network for electric vehicle applications," *International Transactions on Electrical Energy Systems*, vol. 2022, Article ID 2880240, 13 pages, 2022.
[6] R. Ashokkumar, M. Suresh, B. Sharmila et al., "A novel method for Arduino based electric vehicle emulator," *International Journal of Ambient Energy*, vol. 43, no. 1, pp. 4299–4304, 2022.
[7] G. Balan, S. Arumugam, S. Muthusamy et al., "An improved deep learning-based technique for driver detection and driver assistance in electric vehicles with better performance," *International Transactions on Electrical Energy Systems*, vol. 2022, Article ID 8548172, 16 pages, 2022.
[8] G. Chen, Y. Liu, X. Qing, M. Ma, and Z. Lin, "Principle and topology derivation of single-inductor multi-input multi-output DC–DC converters," *IEEE Transactions on Industrial Electronics*, vol. 68, no. 1, pp. 25–36, 2020.
[9] P. KhademiAstaneh, J. Javidan, K. Valipour, and A. Akbarimajd, "A bidirectional high step-up multi-input DC–DC converter with soft switching," *International Transactions on Electrical Energy Systems*, vol. 29, no. 1, Article ID e2699, 2019.
[10] G. Li, J. Xia, K. Wang, Y. Deng, X. He, and Y. Wang, "Hybrid modulation of parallel-series LLC resonant converter and phase shift full-bridge converter for a dual-output DC–DC converter," *IEEE Journal of Emerging and Selected Topics in Power Electronics*, vol. 7, no. 2, pp. 833–842, 2019.
[11] Z. Shen, X. Chang, W. Wang, X. Tan, N. Yan, and H. Min, "Predictive digital current control of single-inductor multiple-output converters in CCM with low cross regulation," *IEEE Transactions on Power Electronics*, vol. 27, no. 4, pp. 1917–1925, 2012.
[12] J. P. V. Ceballos, S. I. Serna-Garcés, D. G. Montoya, C. A. Ramos-Paja, and J. D. Bastidas-Rodríguez, "Charger/discharger DC/DC converter with interleaved configuration for DC-bus regulation and battery protection," *Energy Science & Engineering*, vol. 8, no. 2, pp. 530–543, 2020.
[13] K. Sayed, "Zero-voltage soft-switching DC–DC converter-based charger for LV battery in hybrid electric vehicles," *IET Power Electronics*, vol. 12, no. 13, pp. 3389–3396, 2019.
[14] H. Khalid, S. Mekhilef, M. B. Mubin et al., "Analysis and design of Series-LC-switch capacitor multistage high gain DC–DC boost converter for electric vehicle applications," *Sustainability*, vol. 14, no. 8, Article ID 4495, 2022.
[15] A. Turksoy, A. Teke, and A. Alkaya, "A comprehensive overview of the DC–DC converter-based battery charge balancing methods in electric vehicles," *Renewable and Sustainable Energy Reviews*, vol. 133, Article ID 110274, 2020.
[16] P. S. Tomar, M. Srivastava, and A. K. Verma, "An improved current-fed bidirectional DC–DC converter for reconfigurable split battery in EVs," *IEEE Transactions On Industry Applications*, vol. 56, no. 6, pp. 6957–6967, 2020.
[17] B. Faridpak, M. Farrokhifar, M. Nasiri, A. Alahyari, and N. Sadoogi, "Developing a super-lift Luo-converter with integration of buck converters for electric vehicle applications," *CSEE Journal of Power and Energy Systems*, vol. 7, no. 4, pp. 818–820, 2021.
[18] I. A. Aden, H. Kahveci, and M. E. Şahin, "Design and implementation of single-input multiple-output DC–DC buck converter for electric vehicles," *Journal of Circuits, Systems and Computers*, vol. 30, no. 13, 2021.
[19] D. Yu, J. Yang, R. Xu, Z. Xia, H. H.-C. Iu, and T. Fernando, "A family of module-integrated high step-up converters with dual coupled inductors," *IEEE Access*, vol. 6, pp. 16256–16266, 2018.

[20] S. Song, G. Chen, Y. Liu, Y. Hu, K. Ni, and Y. Wang, "A three-switch-based single-input dual-output converter with simultaneous boost & buck voltage conversion," *IEEE Transactions on Industrial Informatics*, vol. 16, no. 7, pp. 4468–4477, 2020.

[21] S. Saravanan and N. R. Babu, "Design and development of single switch high step-up DC–DC converter," *IEEE Journal of Emerging and Selected Topics in Power Electronics*, vol. 6, no. 2, pp. 855–863, 2018.

[22] F. Ghasemi, M. R. Yazdani, and M. Delshad, "Step-up DC–DC switching converter with single switch and multi-outputs based on Luo Topology," *IEEE Access*, vol. 10, pp. 16871–16882, 2022.